B. KALANDYK*[#], R. ZAPAŁA*, P. PAŁKA**, M. WRÓBEL*

MICROSTRUCTURE AND PROPERTIES OF 17Cr-0.8C CAST STEEL

The results of studies of the microstructure and properties of cast high alloy steels containing 17% Cr and 0.8% C subjected to different variants of heat treatment are presented. For phase identification, the light microscopy and scanning electron microscopy as well as the X-ray diffraction analysis were used. The conducted studies revealed the presence of carbides in the microstructure, mainly of the $M_{23}C_6$ carbide, detected after both quenching and tempering at 200 and 600°C. The use of low and high tempering significantly reduced the test alloy hardness from 657.3 HV_{30} to 403.7 HV_{30}. At the same time, hardness was observed to have an impact on the values of abrasion in the conducted Miller slurry test. Higher material hardness leads to lower wear expressed by mass loss.

Keywords: Martensitic cast steel, $M_{23}C_6$, Fe_7C_3, Fe_3C carbides, Heat treatment, Microstructure, Hardness

1. Introduction

Tool steels and cast tool steels containing 1.0÷1.2% C and 16÷18% Cr belong to the group of most widely used high-quality materials [1-3]. Their numerous applications include, among others, surgical instruments and components operating at temperatures ranging from 0 to 650°C, mainly in the machine industry (bearing parts), metallurgy (CCS mould parts), power engineering (turbine elements) and automotive industry [4-7].

The range of castings made from this alloy includes low-weight precision elements and, owing to the high hardenability, also large castings with heavy cross-sections and varying wall thicknesses.

High content of carbide-forming chromium added to these steels (grades: 440A: 0.6÷0.75% C, 440B: 0.75÷0.95% C, 440C: 0.95÷1.2% C) generates in a ferritic chromium-rich matrix the formation and precipitation of eutectic carbides such as $(Cr,Fe)_{23}C_6$ and $(Cr,Fe)_7C_3$, the effect that largely contributes to a beneficial combination of high strength, hardness and abrasion resistance [2,8-11]. Cast materials can also contain complex phases of the $M_{23}(C,N)_6$ type [3], or nitrides of the Cr_2N type occurring mainly in ferritic and duplex steels [3,8]. Additionally, high chromium content (>12%) makes components cast from these materials more resistant to corrosion [7,8]. The content and the type of carbides present in the steel matrix after heat treatment or after thermo-mechanical treatment will determine the mechanical and functional properties of these alloys [4].

The aim of this study is to discuss the influence of heat treatment on microstructure, hardness and abrasion resistance of cast steel containing 0.8% C and 17.3% Cr.

2. Experimental procedure

The test material was melted in a laboratory 30 kg capacity electric induction furnace. The charge was composed of low-alloy steel scrap, FeCr, FeSi, FeMn, and FeMo. Deoxidation of the melt was carried out with Al and FeSi. Chemical composition of the cast steel melt is shown in Table 1.

TABLE 1

Chemical composition of the investigated cast steel

Materials	C	Mn	Si	P	S	Cr	Mo	other	Fe
	wt. %								
H2÷6	0.8	0.87	0.56	0.005	0.02	17.3	0.22	0.01% Al 0.03% Nb	balance

Y-shaped ingots were cut (50×35×200 mm, without the riser) through and then heat-treated according to the scheme shown in Table 2. Prior to tempering, the samples were held at −70°C for 1 hour. The selection of tempering temperatures is supposed to show how the hardness of the tested steel changes with the temperature change, which is important for tribological applications of the tested material.

* AGH UNIVERSITY OF SCIENCE AND TECHNOLOGY, FACULTY OF FOUNDRY ENGINEERING, 30 MICKIEWICZA AV., 30-059 KRAKOW, POLAND,
** AGH UNIVERSITY OF SCIENCE AND TECHNOLOGY, FACULTY OF NON-FERROUS METALS, 30 MICKIEWICZA AV., 30-059 KRAKOW, POLAND

Corresponding author: bk@agh.edu.pl

Heat treatment of the investigated cast steel

Samples	Type of heat treatment
H2	Q: 1030°C/1500 s/air
H4	Q: 1030°C/1500 s/air + T: 200°C
H6	Q: 1030°C/1500 s/air + T: 600°C

ThermoCalc software was used to simulate solidification of the investigated cast steel. Analysis of the solidification process was performed according to the Scheil-Gulliver model, assuming rapid diffusion in the liquid phase and its absence in the solid phase.

Changes in the microstructure of the investigated cast steel caused by different heat treatment variants were examined under a Neophot 32 light microscope and a Quanta 3D FEG scanning electron microscope equipped with the EDAX energy dispersive X-ray spectrometer for microanalysis of phase chemistry.

Phases occurring in the tested cast steel were identified by X-ray diffraction analysis using a Brucker Discover Advance D8 diffractometer with Cu tube. Due to improved detection of the resulting phases, deep etching of the sample surfaces was performed to „expose" the precipitates in the matrix. Additionally, a Grazing-incidence diffraction technique was used at an angle $\theta = 3°$ and a measurement step of 0.02 degrees. The attack angle q and etching time were chosen in such a way as to provide optimum measurement conditions. The numerical calculations made for a given angle of incidence showed the depth of X-ray penetration for Fe carbides in the range of 0.5÷0.6 μm. For Fe_α it amounted to about 0.47 μm. The adjusted time of etching allowed etching approximately 1mm of the matrix. The selected sample preparation and measurement parameters were aimed at reducing the X-ray attenuation by the matrix.

Hardness tests were performed with a Vickers hardness tester.

Abrasion resistance was examined by the Miller slurry machine tests (ASTM – G75) carried out in a slurry of SiC and water in a ratio of 1:1 [12].

3. Results and discussion

3.1. Simulation of the crystallization process (ThermoCalc)

Simulation of the crystallization process conducted for the test alloy has confirmed the presence of numerous $M_{23}C_6$ carbides in a ferritic matrix in the solid state (Fig. 1). Absence of M_7C_3 carbides in the tested material is probably the result of a lower content of C (Table 1) compared to 440C steels, where the content of this element is ranging from 1.1 to 1.5% C [11]. Although austenite is precipitating from the liquid, and M_7C_3 carbides are formed at 1280°C at the boundaries of austenite grains, further lowering of temperature leads to an increase in the volume fraction of M_7C_3 carbides at the expense of austenite. At a temperature of 1010°C, due to the dissolution of M_7C_3 carbides, the formation of $M_{23}C_6$ carbides begins, and at a temperature of 933°C, only these carbides are present. In the temperature range of 820÷794°C, a eutectoid reaction occurs – austenite is transformed into ferrite, and the content of $M_{23}C_6$ carbides slightly increases, reaching a maximum that persists up to 229°C; then the volume fraction of carbides tends to drop slightly. At a temperature of 322°C, ferrite with lower chromium content is formed.

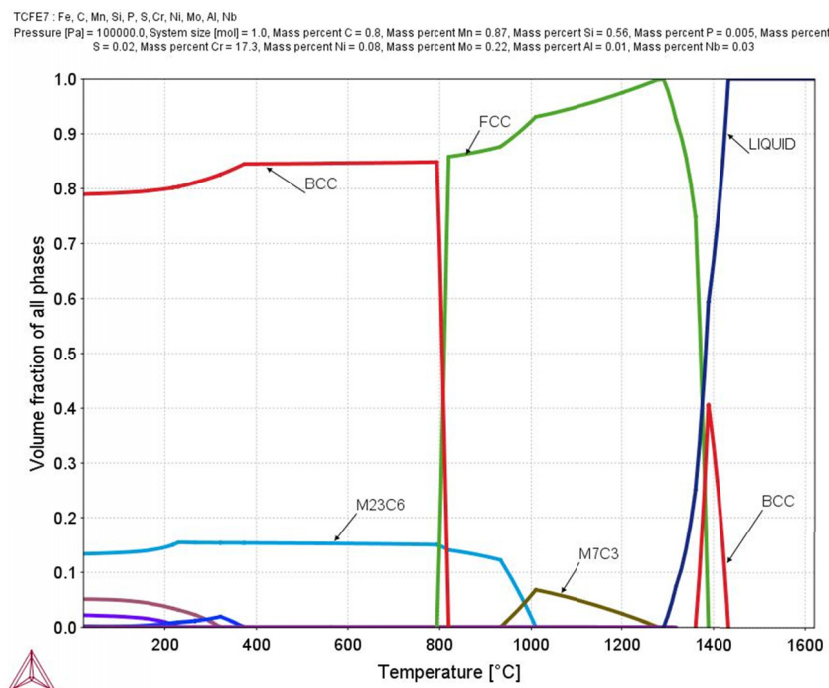The experimental research was based on thermodynamic calculations.

Fig. 1. Equilibrium predicted by ThermoCalc for investigated cast steel
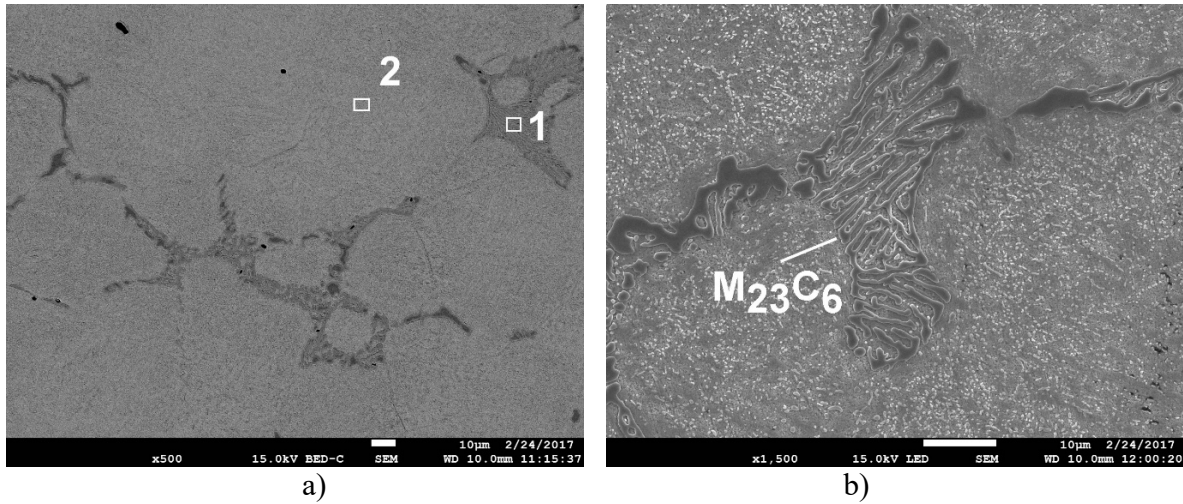
Fig. 2. Microstructure of investigated cast steel – sample H2, discontinuous eutectic carbides network, a) magn. 500×, b) magn. 1500×
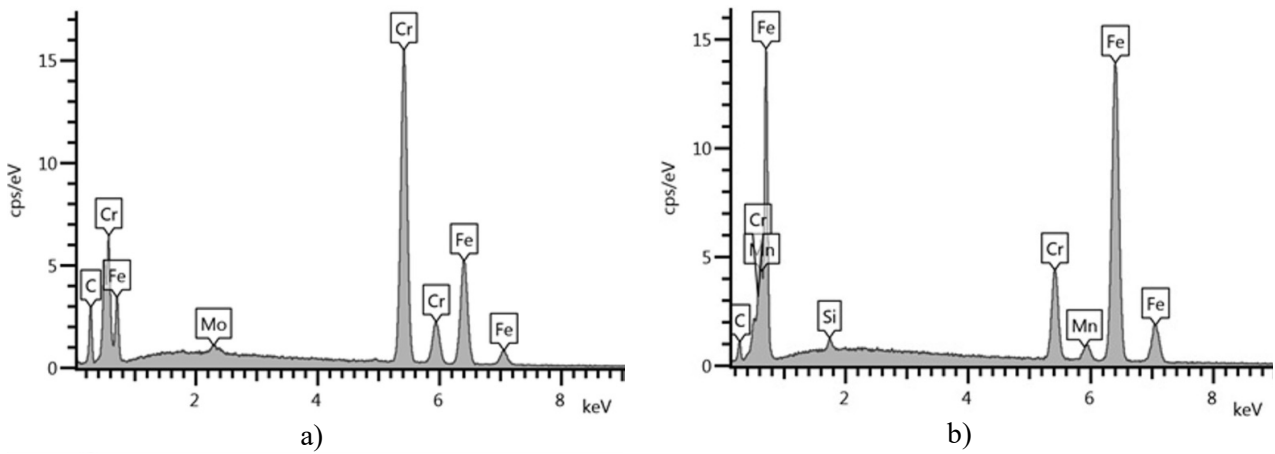

Fig. 3. X-ray diffraction pattern and EDS spectra showing the area of eutectic precipitates in Fig. 2a, area 1 – a) and cast steel matrix in Fig. 2a, area 2 – b)

3.2. Microscopic evaluation

Microstructure of the investigated grade of cast austenitic steel (1030°C/air) is composed of a martensitic matrix and carbide precipitates with two different morphologies. Large eutectic carbides with chromium content higher in respect of the matrix form a network of precipitates at the grain boundaries, while finely dispersed carbides are present inside the grains (Figs. 2,3) [8,11].

Backscattered scanning electron microscopy (BSE) has revealed the heterogeneity of large eutectic precipitates. The areas appearing in light colour contain about 58.8% Cr, 34.7% Fe and 0.8% Mo, while the dark areas contain 66.1% Cr, 24.3% Fe and 0.6% Mo (Fig. 4). Based on the results of microstructural studies of the cast steel, it was found that the light colour precipitates are far more numerous. According to literature [7-11], these precipitates are probably $M_{23}C_6$ and/or M_7C_3 carbides.

Both low and high tempering (i.e. 200°C, 600°C) leaves the microstructure of the investigated cast steel practically unchanged. Eutectic carbide precipitates are still present in the
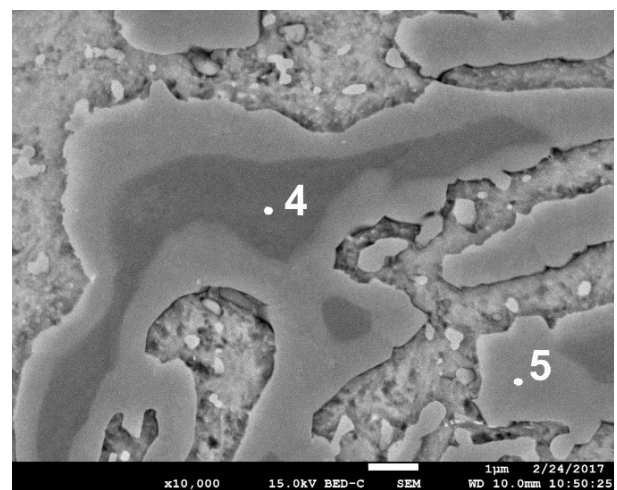
Spectrum Label	C	Cr	Fe	Mo	Total
	wt.%				
Spectrum 4	8.9	66.1	24.4	0.6	100.00
Spectrum 5	5.7	58.8	34.7	0.8	100.00

Fig. 4. Eutectic precipitates in the examined cast steel with microanalysis of chemical composition at points 4 and 5, magn. 10000×
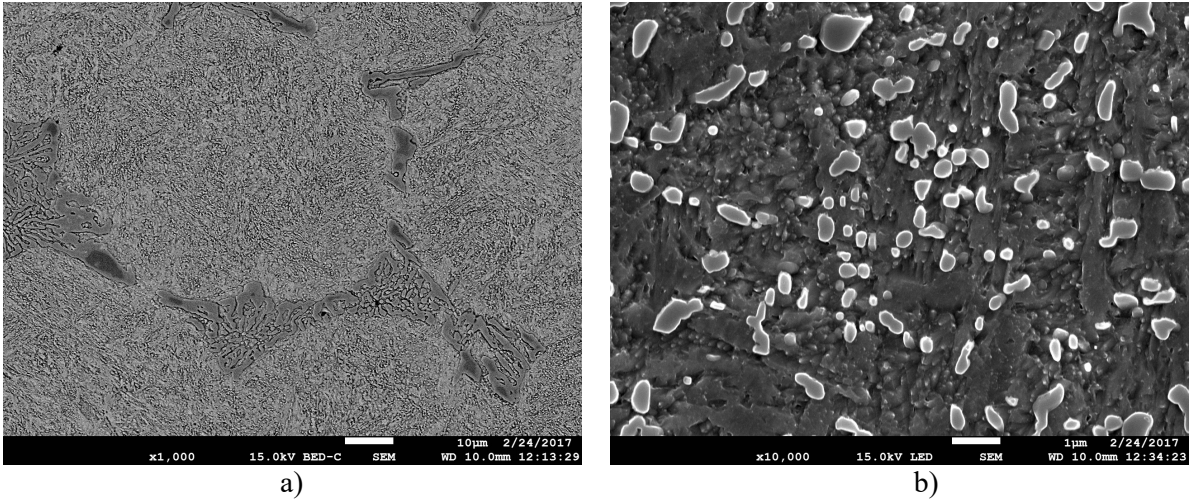
Fig. 5. SEM micrographs, small spherical carbides in matrix investigated cast steel – sample H4 after Q + T: 200°C, a) magn. 1000×, b) magn. 10000×
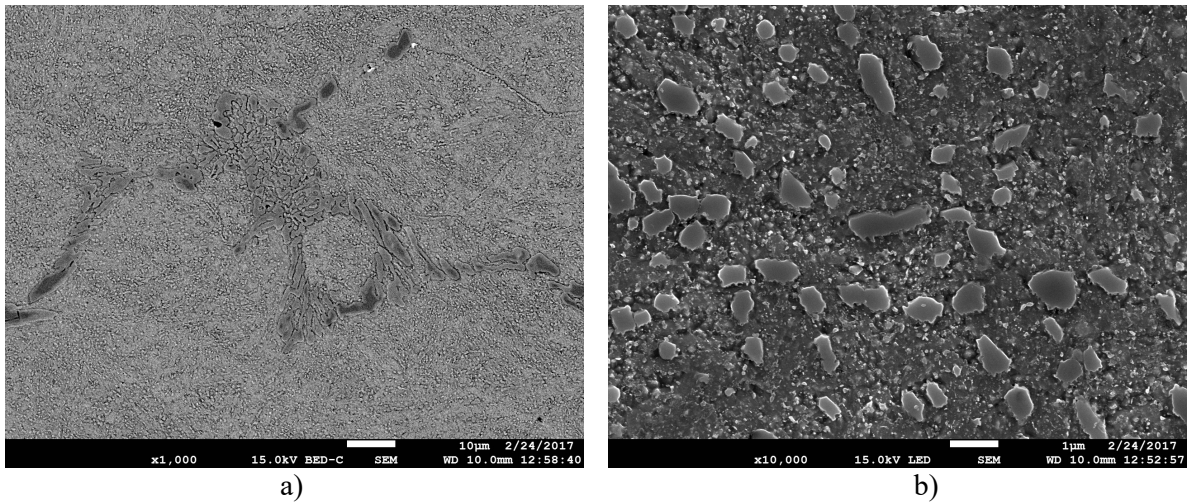

Fig. 6. SEM micrographs, small spherical carbides in matrix investigated cast steel – sample H6 after Q + T: 600°C; a) magn. 1000×, b) magn. 10000×

heterogeneous matrix (Figs. 5,6). Some attention deserves the fact that fine particles present in the matrix and examined at high magnifications (10000×) are larger in size after high tempering (600°C) than after low tempering (Figs. 5b,6b).

Figures 5b and 6b show in the matrix of the examined cast steel the presence of not only fine carbides of the size of about 0.5 μm, but also finely dispersed precipitates of the size of approx. 0.1 μm. The identification of so small precipitates in the matrix requires the use of transmission electron microscopy.

3.3. X- ray diffraction analysis

To identify phases occurring in the test material after low and high tempering, X-ray diffraction analysis was performed. The results are shown in Fig. 7. They confirm the presence of ferrite, which constitutes the alloy matrix, and of $M_{23}C_6$ ($Cr_{15.58}Fe_{7.42}C_6$), Fe_7C_3 and Fe_3C carbides. The presence

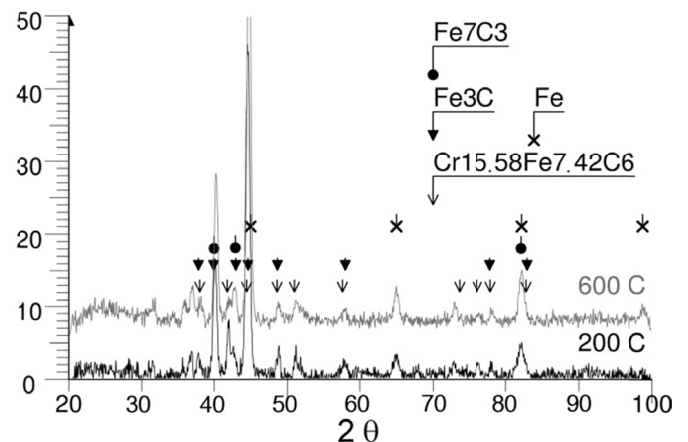of retained austenite was not traced in the recorded X-ray patterns.

Fig. 7. XRD patterns for investigated cast steel after tempering (i.e.: 200, 600°C)

3.4. Hardness

The results of hardness tests after different variants of the heat treatment process are shown in Table 3. As might be expected, increasing the tempering temperature leads to lower hardness (HV_{30}). Compared with hardness after quenching, hardness after tempering assumes lower values.

TABLE 3

Average hardness values (HV_{30}) obtained for the examined cast steel after different variants of the heat treatment

Samples	Hardness HV_{30}
H2	679.3
H4	657.3
H6	403.7

3.5. Miller slurry machine tests

The Miller test made on samples after different variants of the heat treatment has demonstrated a significant difference in the total weight loss of samples after quenching and tempering at 200 and 600°C (Fig. 8). The observed changes corresponded to changes in the sample hardness. The higher was the hardness, the lower was the wear of the test material. Very interesting is the comparable wear rate observed in samples H2 and H4.
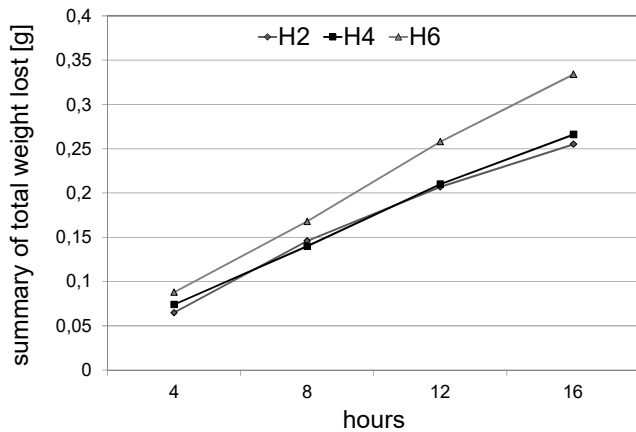

Fig. 8. Changes in the examined cast steel weight during a 16 hour lasting Miller test

4. Conclusions

– The microstructure of the examined cast steel after quenching from 1030°C is mainly composed of eutectic $M_{23}C_6$ carbides containing much higher levels of chromium (58.8÷66.1%) than the matrix (approximately 16.5% Cr). Additionally, the BSE images show that the $M_{23}C_6$ carbide precipitates are not homogeneous (chromium content in the dark areas is higher by about 8÷12%).

– In microstructure of the tested cast steel after tempering (200 and 600°C), apart from the $M_{23}C_6$ carbides, the alloy matrix also contains finely dispersed precipitates whose size increases with the increasing temperature of tempering.

– XRD studies have confirmed the presence of $Cr_{15.58}Fe_{7.42}C_6$, Fe_7C_3 and Fe_3C carbides in the tested cast steel after tempering.

– Increasing the tempering temperature from 200 to 600°C reduces both hardness and abrasion resistance of the examined cast steel.

REFERENCES

[1] Atlas Grade datasheet 440C, http://www.atlas steels.com.au.

[2] http://www.metalravne.co./selector/steels.

[3] D. Peckner, I. Bernstein, Handbook of Stainless Steels, McGraw Hill New York (1977).

[4] J.C. Lippold, D.J. Kotecki, Welding Metallurgy and Weldability of Stainless Steels, Jon Wiley & Sons Inc. (2005).

[5] P.D. Harvey, ASM Metal Park, OH (1982).

[6] K. Clemons, C. Lorraine, G. Salgado, A. Taylor, J. Ogren, P. Umin, et al. Journal of Materials Engineering and Performance **16** (5), 592-596 (2007).

[7] J.R. Yang, T.H. Yu, C.H. Wang, Materials Science and Engineering A **438**, 276-280 (2006).

[8] S. Chenna, N. Kumar Gangwar, K. Abhay Jha, B. Pant, M.G. Koshy, Journal of Materials Engineering and Performance **24** (4), 1656-1662 (2015).

[9] A.A. Salih, M.Z. Omar, S. Junaidi, Z. Sajuri, Australian Journal of Basic Applied Sci. **5** (12), 867-871 (2011).

[10] S.H. Salleh, M.Z. Omar, J. Syarif, M.J. Ghazali, S. Abdullah, Z. Sajuri, Intern. J. of Mechanical Engin. **4** (2), 123-126 (2009).

[11] D. Bombac, M. Fazarinc, A. Saha Podder, G. Kulger, Journal of Materials Engineering and Performance **22** (3), 742-747 (2013). DOI: 10.1007/s11665-012-0340-y.

[12] B. Kalandyk, R. Zapała, Archives od Foundry Engineering **9** (4), 91-94 (2009).